Hindawi Publishing Corporation
BioMed Research International
Volume 2015, Article ID 530957, 11 pages
http://dx.doi.org/10.1155/2015/530957

Research Article

Effect of Fe_3O_4 Nanoparticles on Skin Tumor Cells and Dermal Fibroblasts

Lirija Alili,[1] Swetlana Chapiro,[1] Gernot U. Marten,[2] Annette M. Schmidt,[2] Klaus Zanger,[3] and Peter Brenneisen[1]

[1]*Institute of Biochemistry & Molecular Biology I, Medical Faculty, Heinrich Heine University, 40225 Düsseldorf, Germany*
[2]*Department of Chemistry, Institute of Physical Chemistry, University of Cologne, 50939 Cologne, Germany*
[3]*Institute of Anatomy II, Medical Faculty, Heinrich Heine University, 40225 Düsseldorf, Germany*

Correspondence should be addressed to Lirija Alili; lirija.alili@web.de

Received 16 January 2015; Accepted 24 February 2015

Academic Editor: Narinder Singh

Iron oxide (Fe_3O_4) nanoparticles have been used in many biomedical approaches. The toxicity of Fe_3O_4 nanoparticles on mammalian cells was published recently. Though, little is known about the viability of human cells after treatment with Fe_3O_4 nanoparticles. Herein, we examined the toxicity, production of reactive oxygen species, and invasive capacity after treatment of human dermal fibroblasts (HDF) and cells of the squamous tumor cell line (SCL-1) with Fe_3O_4 nanoparticles. These nanoparticles had an average size of 65 nm. Fe_3O_4 nanoparticles induced oxidative stress via generation of reactive oxygen species (ROS) and subsequent initiation of lipid peroxidation. Furthermore, the question was addressed of whether Fe_3O_4 nanoparticles affect myofibroblast formation, known to be involved in tumor invasion. Herein, Fe_3O_4 nanoparticles prevent the expression alpha-smooth muscle actin and therefore decrease the number of myofibroblastic cells. Moreover, our data show *in vitro* that concentrations of Fe_3O_4 nanoparticles, which are nontoxic for normal cells, partially reveal a ROS-triggered cytotoxic but also a pro-invasive effect on the fraction of squamous cancer cells surviving the treatment with Fe_3O_4 nanoparticles. The data herein show that the Fe_3O_4 nanoparticles appear not to be adequate for use in therapeutic approaches against cancer cells, in contrast to recently published data with cerium oxide nanoparticles.

1. Introduction

Besides an anchorage-independent cell proliferation an important, still treatment-limiting characteristic of malignant tumors is their ability for invasive and metastatic growth [1, 2]. During the invasion process, interactions of tumor cells with the neighbouring interstitial stroma, which is composed of fibroblastic, myofibroblastic, endothelial, and inflammatory cells, as well as extracellular matrix components, play a pivotal role [3, 4]. Molecular mechanisms of tumor-stroma interactions include the secretion of multiple growth factors and cytokines by tumor cells and activated stromal cells which stimulate tumor invasion, tumor development, and neoangiogenesis [5]. Myofibroblasts are modified fibroblasts that express the biomarker alpha-smooth muscle actin (αSMA) [6]. The myofibroblastic cell type was originally described in the physiological process of wound healing where it contracts the stroma thereby facilitating wound closure [7, 8]. Meanwhile, it is well known that myofibroblasts are also involved in pathological processes and diseases like fibrosis and cancer [9]. They contribute to tumor progression and are, therefore, often found at the tumor invasion front [10–12]. The interaction between myofibroblasts and cancer cells is dependent on proinvasive growth-promoting factors through paracrine effects [13]. The transition of fibroblasts to myofibroblasts is primarily initiated by transforming growth factor β1 (TGFβ1) [14] and mediated through Smad protein-dependent as well as Smad independent pathways [15]. Previously, we showed that TGFβ1 induces a reactive oxygen species- (ROS-) mediated pathway leading to formation of myofibroblasts via involvement of protein kinase C (PKC) [16] and NAD(P)H oxidase [17].

Nanoparticles are generally defined as structures with sizes between 1 and 100 nm that have a very large surface-to-volume ratio leading to different, novel properties compared with bulk particles of the same chemical composition [18, 19]. Because of their unique features and the fact that such nanoscale materials are small enough to enter cells and organelles [20, 21], nanoparticles are used for many biomedical approaches *in vitro* and *in vivo* [22]. One example for iron oxide nanoparticle based cancer therapy would be the magnetic fluid hyperthermia therapy (MFH) [23]. Injected magnetic iron oxide nanoparticles are heated by an alternating magnetic field leading to tumor cell death either through apoptosis or necrosis [24, 25]. Although iron oxide nanoparticles are increasingly used for medical purposes, the actual intracellular influence of these structures is not clear till now. As consequence of the increased surface-to-volume ratio, nanoparticles exhibit a potentially higher biological activity compared with larger particles which has been linked to prooxidative but also to antioxidative processes [26–31]. The aim of this study was to determine cell toxicity, myofibroblast development, and tumor invasion, after treatment with Fe_3O_4 nanoparticles.

2. Materials and Methods

Cell culture media (Dulbecco's modified Eagle's medium (DMEM)) were purchased from Invitrogen (Karlsruhe, Germany) and the defined fetal calf serum (FCS gold) was from PAA Laboratories (Linz, Austria). All chemicals including protease as well as phosphatase inhibitor cocktail 1 and 2 were obtained from Sigma (Taufkirchen, Germany) or Merck Biosciences (Bad Soden, Germany) unless stated otherwise. The protein assay kit (Bio-Rad DC, detergent compatible) was from Bio-Rad Laboratories (München, Germany). Matrigel and polycarbonate cell culture inserts (6.5 mm diameter, 8 μm pore size) were delivered from BD Biosciences (Heidelberg, Germany). The Oxyblot Protein Oxidation Detection Kit was from Millipore (Schwalbach, Germany). The enhanced chemiluminescence system (Super-Signal West Pico/Femto Maximum Sensitivity Substrate) was supplied by Pierce (Bonn, Germany). Monoclonal mouse antibodies raised against human α-smooth muscle actin and α-tubulin were supplied by Sigma. The following secondary antibodies were used: polyclonal horseradish peroxidase-(HRP-) conjugated rabbit anti-mouse IgG antibody (DAKO, Glostrup, Denmark) and goat anti-rabbit immunoglobulin G antibodies were from Dianova (Hamburg, Germany). Recombinant human TGFβ1 (rTGFβ1) was from R&D Systems (Wiesbaden, Germany).

2.1. Cell Culture. Human dermal fibroblasts (HDF) were established by outgrowth from foreskin biopsies of healthy human donors with an age of 3–6 years. Cells were used in passages 2–12, corresponding to cumulative population doubling levels of 3–27 [32]. Dermal fibroblasts and the squamous carcinoma cell line SCL-1, originally derived from the face of a 74-year-old woman [33] (generously provided by Professor Dr. Norbert Fusenig, DKFZ Heidelberg, Germany), were cultured as described [34]. Myofibroblasts (MF) were generated by treatment of HDF with recombinant TGFβ1 (rTGFβ1) for 48 h in conditioned medium from HDF (CM^{HDF}) [16].

2.2. Preparation of Conditioned Medium. Conditioned medium was obtained from human dermal fibroblasts (CM^{HDF}) and myofibroblasts (CM^{MF}). For this, seeded 1.5×10^6 HDF cells were grown to subconfluence (~70% confluence) in 175 cm^2 culture flasks. The serum-containing medium was removed, and after washing in phosphate-buffered saline (PBS) the cells were incubated in serum-free DMEM or treated with rTGFβ1 (5 ng/mL) in serum-free DMEM for 48 hours. This medium was removed, and after washing in PBS all cells were incubated in 15 mL serum-free DMEM for further 48 hours before collection of the now called conditioned medium of HDF (CM^{HDF}) and myofibroblasts ($CM^{HDF,TGF\beta1} = CM^{MF}$). Conditioned media were used fresh or stored at −20°C for at the most 2 weeks before use [30].

2.3. Synthesis and Stabilization of Fe_3O_4 Nanoparticles. The synthesis of magnetite nanoparticles on the gram scale was carried out by alkaline precipitation of iron(III) and iron(II) chloride following a method of Cabuil and Massart as described in detail elsewhere [35]. For stabilization, the freshly synthesized nanoparticles were stirred with 420 mL of 2 N nitric acid for 5 min. After washing with distilled water, 90 mL 0.01 N citric acid (CA) was added to the nanoparticles and stirred for 5 min. The particles were magnetically separated from the supernatant and 15 mL of tetramethylammonium hydroxide aqueous solution was added to obtain 3.32 g magnetic nanoparticles Fe_3O_4@CA in 92 mL of a stable dispersion at pH 8-9 (yield: 42.5%). The Fe_3O_4 content $\mu(Fe_3O_4)$ in dispersion and the magnetic core diameter d_c were determined via Vibrating Sample Magnetometer (VSM) ($\mu(Fe_3O_4) = 2.55$ mass%, $d_c = 11.7$ nm). DLS: $d_{h,n} = 14.3$ nm (25°C in H_2O). Fourier transform infrared spectroscopy (FTIR) (Diamond): ν (cm^{-1}) = 2357, 2335 (C–N), 1247 (OH), 1098 (C–O), and 1080 (OH) [36].

2.4. Surface Modification of Fe_3O_4 Nanoparticles. For the immobilization of initiator sites on the particle surface of Fe_3O_4@CA, the dispersion was diluted with ethanol to a mass content of 1.0 g·l^{-1}, and 1.80 mmol 4-(chloromethyl) phenyltrimethoxysilane (CTS) per gram of Fe_3O_4 was added. After stirring for 24 h at ambient temperature, ethanol was removed under reduced pressure at 40°C and the particles were washed with ethanol/acetone (1 : 1) five times. The particles were then redispersed in DMSO, resulting in a Fe_3O_4 content $\mu(Fe_3O_4)$ of 6.44 mass % (VSM) in dispersion (yield: 46.4%). The magnetic core diameter d_c was measured to be 11.1 nm (VSM). The functionalization degree of CPS was determined by EA to be 0.87 mmol CTS on 1.94 g Fe_3O_4@CPS. FT-IR (Diamond): ν (cm^{-1}) = 2357, 2335 (C–N), 1241 (OH), 1115 (Si–O), 1011, and 948 (Si–C) [36].

2.5. Surface-Initiated Atom Transfer Radical Polymerization (ATRP) of Functional Polymer Shells. The obtained CPS

coated particles served as a macroinitiator for the following ATRP. The synthesis of Fe_3O_4@P(O_{100}) is described, representatively. Therefore 6 mL of the DMSO-based particle dispersion (0.65 g Fe_3O_4@CPS) was mixed with 5 mL of a DMSO solution of 37.3 mg (0.26 mmol) CuBr and 101 mg (0.65 mmol) 2,2-bipyridine (bpy). The polymerization was started by adding 5.83 mmol of the monomer (here: oligo(ethylene glycol) methylether methacrylate (OEGMA)). The mixture was stirred for 24 h at ambient temperature. The obtained viscous magnetic fluid was diluted with 10 mL DMSO to the final ferrofluid. The Fe_3O_4 content $\mu(Fe_3O_4)$ in dispersion and the magnetic core diameter d_c were determined via VSM. The polymer content χ_{Pol} in the dried particles was obtained from elemental analysis (EA) and thermogravimetric analysis (TGA) [36].

2.6. Particle Transfer to Water/Buffer. The DMSO-based particle dispersion was added dropwise to diethyl ether (Et_2O). The precipitate was washed five times with Et_2O/acetone (1 : 1) and was redispersed in distilled water or buffer to obtain an aqueous magnetic fluid [36].

2.7. Cell Viability. The cytotoxic effect of Fe_3O_4 nanoparticles was measured by MTT (3-(4,5-dimethylthiazol-2-yl)-2,5-diphenyltetrazolium bromide) assay [37]. The activity of mitochondrial dehydrogenases, as indicator of cellular viability, results in formation of a purple formazan dye. Briefly, MTT solution (0.5 mg/mL) was added to the cells treated with different concentrations of Fe_3O_4 nanoparticles after washing with PBS. Cells were incubated for an additional 20 min. The medium was removed and the cells were lysed in dimethyl sulfoxide. The formazan formation was measured at 570 nm. The results were presented as percentage of untreated control which was set at 100%.

2.8. Cellular Uptake of Nanoparticles. Human dermal fibroblasts (HDF) and squamous cancer cells (SCL-1) in serum-free Dulbecco's Modified Eagle Medium (DMEM) were treated with 350 μM Fe_3O_4 nanoparticles for 24 h. Thereafter, cells were harvested and washed with phosphate-buffered saline (PBS) to remove excess media. As the nanoparticles are not detectable by phase contrast microscopy, transmission electron microscopy was used to determine the cellular uptake of Fe_3O_4 nanoparticles. For electron microscopy, pelleted samples of Fe_3O_4 nanoparticles-treated cells were fixed for 2 h in 4% paraformaldehyde and 2.5% glutaraldehyde (Serva, Heidelberg, Germany) in 0.1 M phosphate buffer at pH 7.4 at room temperature. Next, the pellets were thoroughly washed with four changes of PBS, followed by a postfixation for 60 min in 1% osmium tetroxide (Serva) in PBS. The specimens were dehydrated in a graded series of acetone and embedded in Spurr's medium (Serva) at 70°C for 24 h.

Ultrathin sections were cut from the embedded tissue with a Reichert Ultracut (Vienna, Austria) using a diamond knife. The sections were collected on coated copper grids and subsequently stained with uranyl acetate and lead citrate according to earlier published data [38]. The grids were analyzed using a Hitachi H 600 electron microscope (Düsseldorf, Germany). Documentation was carried out by using an optical system and the Digital Micrograph software (Gatan, Munich, Germany). For light microscopical controls semithin sections were cut and stained with 1% Toluidine blue and 1% Borax [30].

2.9. SDS-PAGE and Western Blotting. SDS-PAGE was performed according to the standard protocols published elsewhere [39] with minor modifications. Briefly, cells were lysed after incubation with Fe_3O_4 nanoparticles in 1% SDS with 1 : 1000 protease inhibitor cocktail (Sigma; Taufkirchen, Germany). After sonication, the protein concentration was determined by using a modified Lowry method (Bio-Rad DC). 4x SDS-PAGE sample buffer (1.5 M Tris-HCl pH 6.8, 6 mL 20% SDS, 30 mL glycerol, 15 mL β-mercaptoethanol, and 1.8 mg bromophenol blue) was added, and after heating, the samples (20–30 μg total protein/lane) were applied to 8% (w/v) SDS-polyacrylamide gels. After electroblotting, immunodetection was carried out (1 : 1000 dilution) of primary antibodies (rabbit monoclonal anti-HIF1α and mouse monoclonal anti-α-tubulin), 1 : 20000 dilution of anti-mouse/rabbit antibody conjugated to HRP). Antigen-antibody complexes were visualized by an enhanced chemiluminescence system. α-tubulin was used as internal control for equal loading.

2.10. Invasion Assay. Cell culture inserts (transwells) were overlaid with 125 μg/mL growth factor-reduced matrigel and placed in a 24-well plate. Tumor cells (5×10^4 cells/insert) either untreated or pretreated with Fe_3O_4 nanoparticles were seeded on top of the matrigel in serum-free DMEM. Conditioned medium of human dermal fibroblasts (CM^{HDF}) or of myofibroblasts (CM^{MF}) (see above) was used as chemoattractant in the lower chamber. After 30 h at 37°C, the melanoma cells were rubbed off the upper side of the filter using cotton swabs, and the tumor cells, which invaded to the lower side of the insert, were stained with Coomassie Blue solution (0.05% Coomassie Blue, 20% MeOH, and 7.5% acetic acid). The number of invaded cells was estimated by counting 25 random microscopic fields/insert [16, 30].

2.11. Determination of Oxidized (Carbonylated) Proteins: Oxyblot Analysis. Tumor cells were grown to subconfluence on tissue culture dishes. After removal of serum-containing medium, cells were cultured in serum-free medium and either untreated or pretreated for different times with 350 μM Fe_3O_4 nanoparticles. As positive control, the cells were treated with 250 μM H_2O_2. Thereafter, cells were lysed and carbonyl groups of oxidized proteins were detected with the OxyBlot Protein Oxidation Detection Kit, following the manufacturer's protocol. Briefly, the protein concentration was determined by using a modified Lowry method (Bio-Rad DC). The protein amounts of the samples were aligned. Five μg of this cell lysate was incubated with 2,4-dinitrophenyl (DNP) hydrazine to form the DNP hydrazone derivatives. Labeled proteins were separated by SDS-PAGE and immunostained using rabbit anti-DNP antiserum (1 : 500) and goat anti-rabbit IgG conjugated to horseradish peroxidase (1 : 2000). Blots were developed by enhanced chemiluminescence.

2.12. Enzyme-Linked Immunosorbent Assay (ELISA). By means of the ELISA method, the content of 8-iso prostaglandin F2α (8-PGF2a isopropyl, 8-isoprostane) was investigated in cell culture supernatants from SCL-1 cells. The assay was performed using the Acetylcholinesterase Competitive Enzyme Immunoassay kit (Cayman Chemical, Michigan, USA) according to the manufacturer's instructions. This assay is based on the competition between 8-isoprostane and an 8-isoprostane-acetylcholinesterase (AChE) conjugate (8-isoprostane tracer) for a limited number of 8-isoprostane-specific rabbit antiserum binding sites. Because the concentration of the 8-isoprostane tracer is held constant while the concentration of 8-isoprostane varies, the amount of 8-isoprostane tracer that is able to bind to the rabbit antiserum will be inversely proportional to the concentration of 8-isoprostane in the well. This rabbit antiserum-8-isoprostane (either free or tracer) complex binds to the rabbit IgG mouse monoclonal antibody that has been previously attached to the well. The plate is washed to remove any unbound reagents and then Ellman's Reagent (which contains the substrate to AChE) is added to the well. The product of this enzymatic reaction has a distinct yellow color and absorbs strongly at 412 nm. The intensity of this color, determined spectrophotometrically, is proportional to the amount of 8-isoprostane.

2.13. Determination of Malondialdehyde (MDA). MDA is a marker of lipid peroxidation and was determined by HPLC [40] after derivatization with 2-thiobarbituric acid [41]. The HPLC system consisted of a Merck Hitachi L-7100 pump connected with a Merck fluorescence detector (Merck Hitachi; FL Detector L-7480) and a data registration system. Analyses were performed isocratically with a mobile phase composed of 60% phosphate buffer (NaH_2PO_4/Na_2HPO_4 buffer; 50 mmol/L; pH 6.5) and 40% methanol (v/v) at a flow rate of 1 mL/min and a reversed-phase column (LiChrospher 100 RP18, 5 μm; Merck) protected by a guard column (4.6 × 4.6 mm) of the same stationary phase. Excitation wavelength was 513 nm and emission wavelength 550 nm. MDA levels were calculated by external calibration with 1,1,3,3-tetramethoxypropane, which releases a stoichiometric amount of MDA in an acidic solution. The MDA amount was normalized to the protein content [42].

2.14. Statistical Analysis. Means were calculated from at least three independent experiments, and error bars represent standard error of the mean (s.e.m.). Analysis of statistical significance was done by Student's t-test or ANOVA with $^{*}p < 0.05$, $^{**}p < 0.01$, and $^{***}p < 0.001$ as levels of significance.

3. Results

Herein, the effect of Fe_3O_4 nanoparticles in tumor-stroma interaction was studied. We investigated the influence of Fe_3O_4 nanoparticles in cultured human dermal fibroblasts and on human squamous carcinoma cells (SCL-1). Fe_3O_4 nanoparticles are nontoxic on stromal cells (e.g., fibroblasts) but the cell viability in tumor cells was significantly lowered. Oxidative stress parameters, for example, total reactive oxygen species, carbonylated proteins, and formation of malondialdehyde, were investigated.

3.1. Cell Viability. The potential toxicity of Fe_3O_4 nanoparticles on human dermal fibroblasts (HDF) was tested. The fibroblasts were incubated with 65 nm-sized polymer-coated Fe_3O_4 nanoparticles for 72 h. MTT assays were used to analyze the viability of the cells. Cell viability was evidently not altered after 72 h for these cells (Figure 1(a)).

3.2. Cellular Uptake of Fe_3O_4 Nanoparticles. The cellular uptake of Fe_3O_4 nanoparticles was examined by the use of transmission electron microscopy (TEM). Figure 1(b) shows the TEM micrographs of human dermal fibroblasts (A, B) and SCL-1 tumor cells (C, D). After treatment of the cells for 24 h with nanoparticles the TEM micrographs of the cells show Fe_3O_4 nanoparticles as solid black dots (see arrows) localized in the cytosol (B, D) compared to untreated controls (A, C) (Figure 1(b)). However, the incorporated Fe_3O_4 nanoparticles are at least in part agglomerated in the cells.

3.3. Effect of Fe_3O_4 Nanoparticles on Myofibroblast Development. We studied the effect of Fe_3O_4 nanoparticles on αSMA mRNA level in human dermal fibroblasts using real-time RT-PCR. The "housekeeping" gene HPRT was used as internal control. The αSMA mRNA level increased 14 ± 4-fold after 24 h treatment of rTGFβ1 compared to untreated controls. Pretreatment with Fe_3O_4 nanoparticles significantly lowered the rTGFβ1 mediated transcription of αSMA mRNA by 50% (50 μM Fe_3O_4) and by 75% (350 μM Fe_3O_4) (Figure 2(a)). These data correlated with the αSMA protein amount (Figure 2(b)). The αSMA protein level was lowered by 50% after preincubation with 350 μM Fe_3O_4 nanoparticles (Figure 2(b)).

3.4. Fe_3O_4 Nanoparticles in Squamous Tumor Cells. Figure 3(a) displays the result of the MTT assay of SCL-1 cells after incubation with Fe_3O_4 nanoparticles for 72 h. 350 μM Fe_3O_4 nanoparticles killed tumor cells significantly to 50% but had no toxic effect on the viability of dermal fibroblasts (see Figure 1(a)). These results suggest that Fe_3O_4 nanoparticles select between tumor and healthy cells. Therefore it may be used in chemoprevention of squamous tumor cells. The SCL-1 cells which persisted after treatment with 350 μM Fe_3O_4, reflect the data of the invasion assays.

3.5. Involvement of Fe_3O_4 Nanoparticles on Invasive Capacity of Tumor Cells. Myofibroblasts (MF) affect the invasion of tumor cells [16]. Antioxidants inhibit the expression of alpha-smooth muscle actin resulting in prevention of myofibroblast formation [16]. Herein, we checked if Fe_3O_4 nanoparticles modulate the invasive capacity of tumor cells. Fe_3O_4 nanoparticles treatment inhibits the myofibroblast formation. Conditioned media (CM) of HDF treated with TGFβ1 and Fe_3O_4 nanoparticles (CM^{HDF,TGF,Fe_3O_4}) were used to check the invasive capacity of tumor cells (Figure 3(b)). The invasion of the squamous tumor cells was 30–50% lowered by

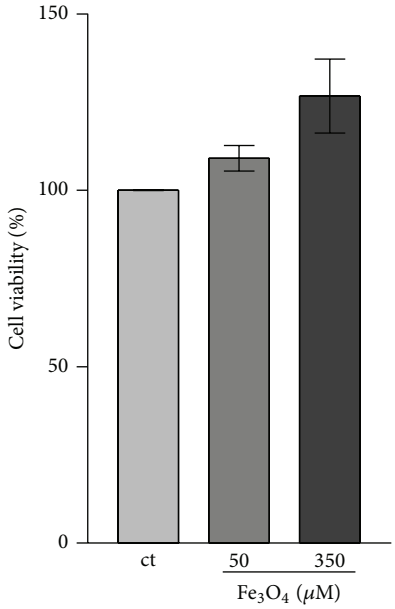

(a)

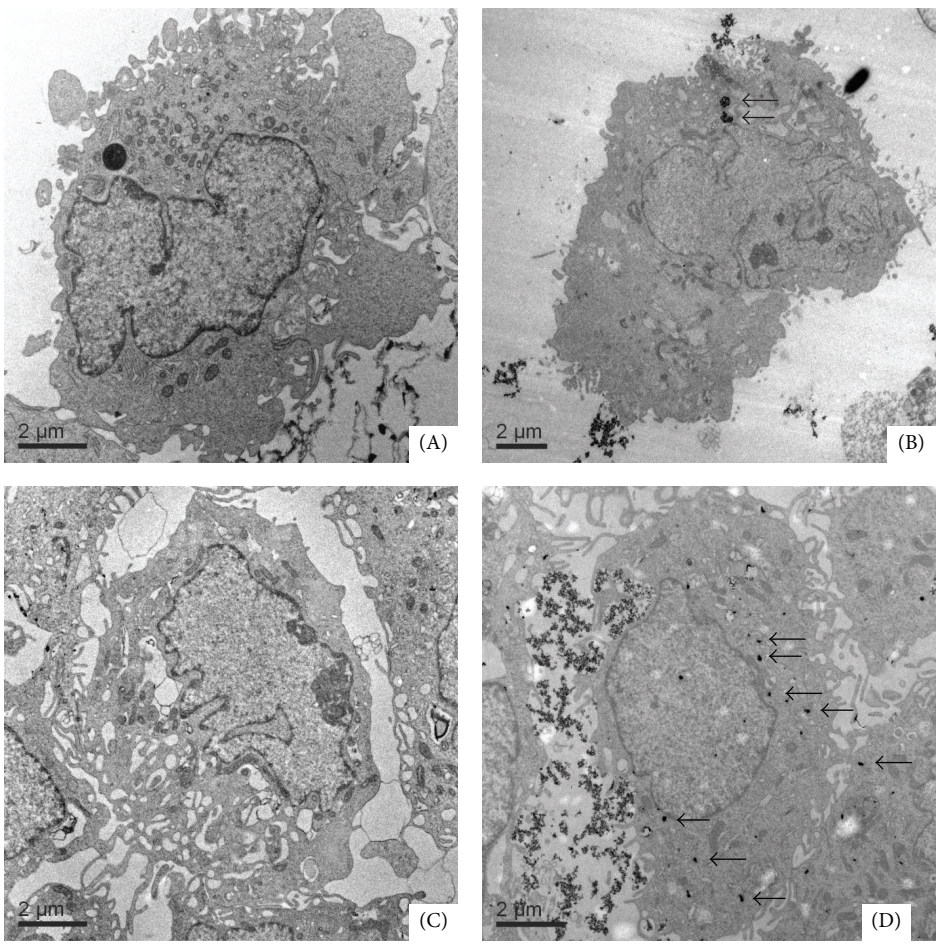

(b)

Figure 1: (a) Cell viability of fibroblasts. Cells were incubated with Fe_3O_4 nanoparticles. The percentage of living cells was measured after 72 h. $n = 3$. (b) Cellular uptake of Fe_3O_4 nanoparticles. Fibroblasts (HDF) (A, B) and SCL-1 tumor cells (C, D) were untreated (A, C) or incubated (B, D) with 350 μM Fe_3O_4 nanoparticles for 24 h to determine the cellular uptake of the nanoparticles.

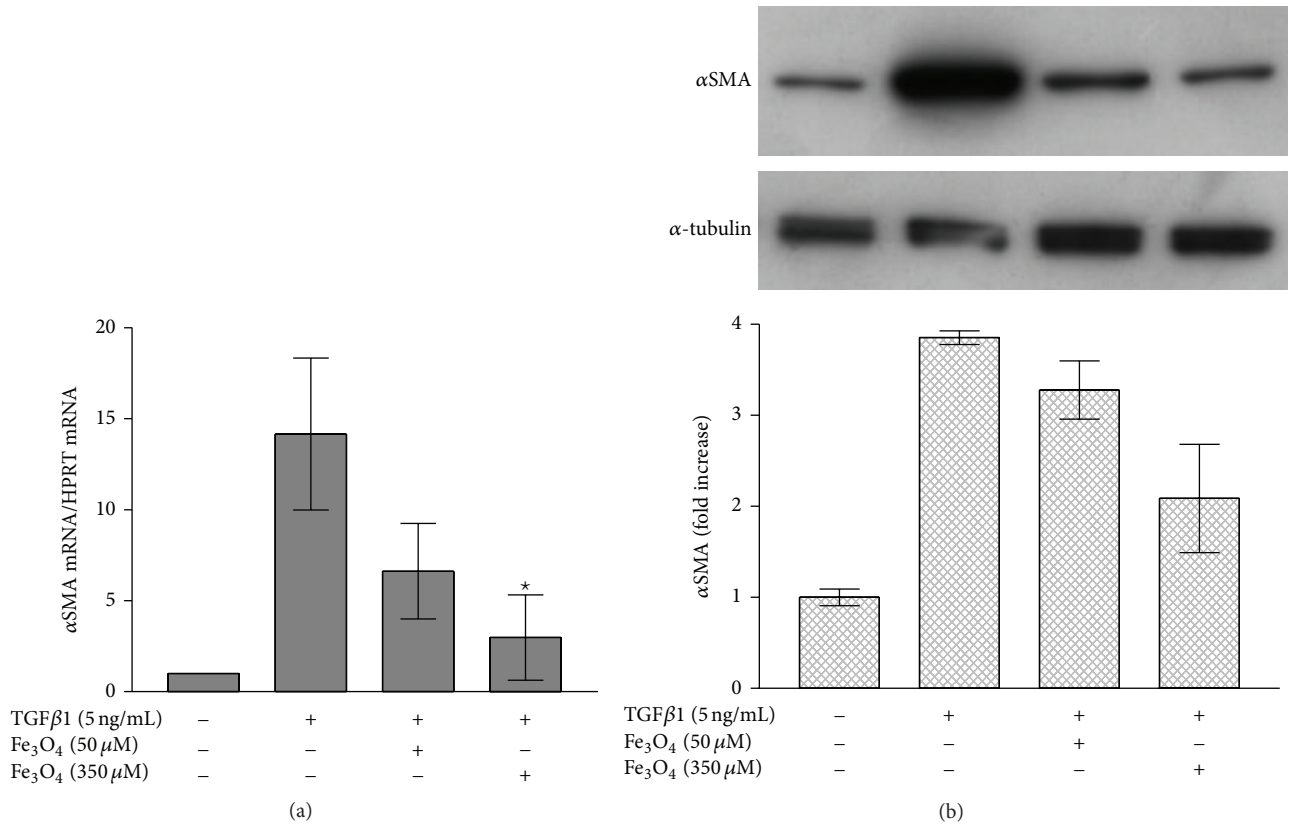

Figure 2: Effect of Fe_3O_4 nanoparticles on myofibroblast formation. (a) Gene expression of αSMA was analyzed by real-time RT-PCR with normalization against HPRT1. The data represent means ± s.e.m. $n = 3$. CM: conditioned medium. $^*p < 0.05$ versus TGFβ1 treatment only (Student's t-test). (b) Fibroblasts were grown to subconfluence. These cells were either untreated or incubated with 50 μM or 350 μM Fe_3O_4 nanoparticles for 24 h before treatment with rTGFβ1. TGFβ1 and the Fe_3O_4 nanoparticles were present for 48 h. α-tubulin served as loading control. $n = 3$. CM: conditioned medium.

using CM^{HDF,TGF,Fe_3O_4} compared with $CM^{HDF,TGF}$. Additionally, the direct effect of Fe_3O_4 nanoparticles on tumor cells was studied. Therefore, the fibroblasts were not incubated with Fe_3O_4 nanoparticles. We used the conditioned medium (CM) of fibroblasts (CM^{HDF}) and myofibroblasts (CM^{MF}). SCL-1 tumor cells were incubated with 350 μM Fe_3O_4 nanoparticles. After 48 h the invasion of the tumor cells was checked. Untreated cells were used as control (Figure 3(c)). Surprisingly, Fe_3O_4 nanoparticles significantly increased the invasive capacity by 50% using both CM^{HDF} and CM^{MF}. In that context, the direct treatment of SCL-1 tumor cells with cerium oxide nanoparticles showed the opposite effect [30]. In conclusion, even though the prevention of myofibroblast formation by Fe_3O_4 nanoparticles resulted in downregulation of tumor invasion, the direct treatment of the SCL-1 cells with the Fe_3O_4 nanoparticles increased the invasive capacity.

3.6. Reactive Oxygen Species and Carbonylated Proteins. ROS generation plays a great role in cellular viability and invasive capacity of cells. To check whether our results with Fe_3O_4 nanoparticles are due to ROS production, we performed a western blot. This special blot detects carbonylated (oxidized) proteins, which is a biomarker for intracellular oxidative stress [43]. SCL-1 tumor cells were incubated with Fe_3O_4 nanoparticles for 24 h and the oxyblot was performed. Untreated SCL-1 cells showed a low amount of oxidized proteins. However, H_2O_2- and Fe_3O_4-treatment significantly increased the amount in tumor cells (Figure 4(a)). The maximum of the level of oxidized proteins was identified after treatment with 350 μM Fe_3O_4 nanoparticles with a 5.5-fold increase.

3.7. Formation of 8-Isoprostane by Fe_3O_4 Nanoparticles. Furthermore, an important parameter for oxidative stress, the lipid peroxidation, was examined [44]. After treatment of the squamous tumor cells with Fe_3O_4 nanoparticles, 8-isoprostane, one of several end products of lipid peroxidation, was detected in the cell culture supernatant. The isoprostanes are a family of eicosanoids of nonenzymatic origin produced by the random oxidation of tissue phospholipids by oxygen radicals (8-Isoprostane EIA Kit, Cayman Chemical, Michigan, USA). They are considered as best *in vitro* and *in vivo* markers for oxidative stress and antioxidant deficiency [45, 46]. The content of 8-isoprostane in the supernatant of tumor cells treated with Fe_3O_4 compared with untreated control cells is shown in Figure 4(b).

After 4 h of incubation with 50 μM Fe_3O_4 nanoparticles, no increase of 8-isoprostane in the culture supernatants of

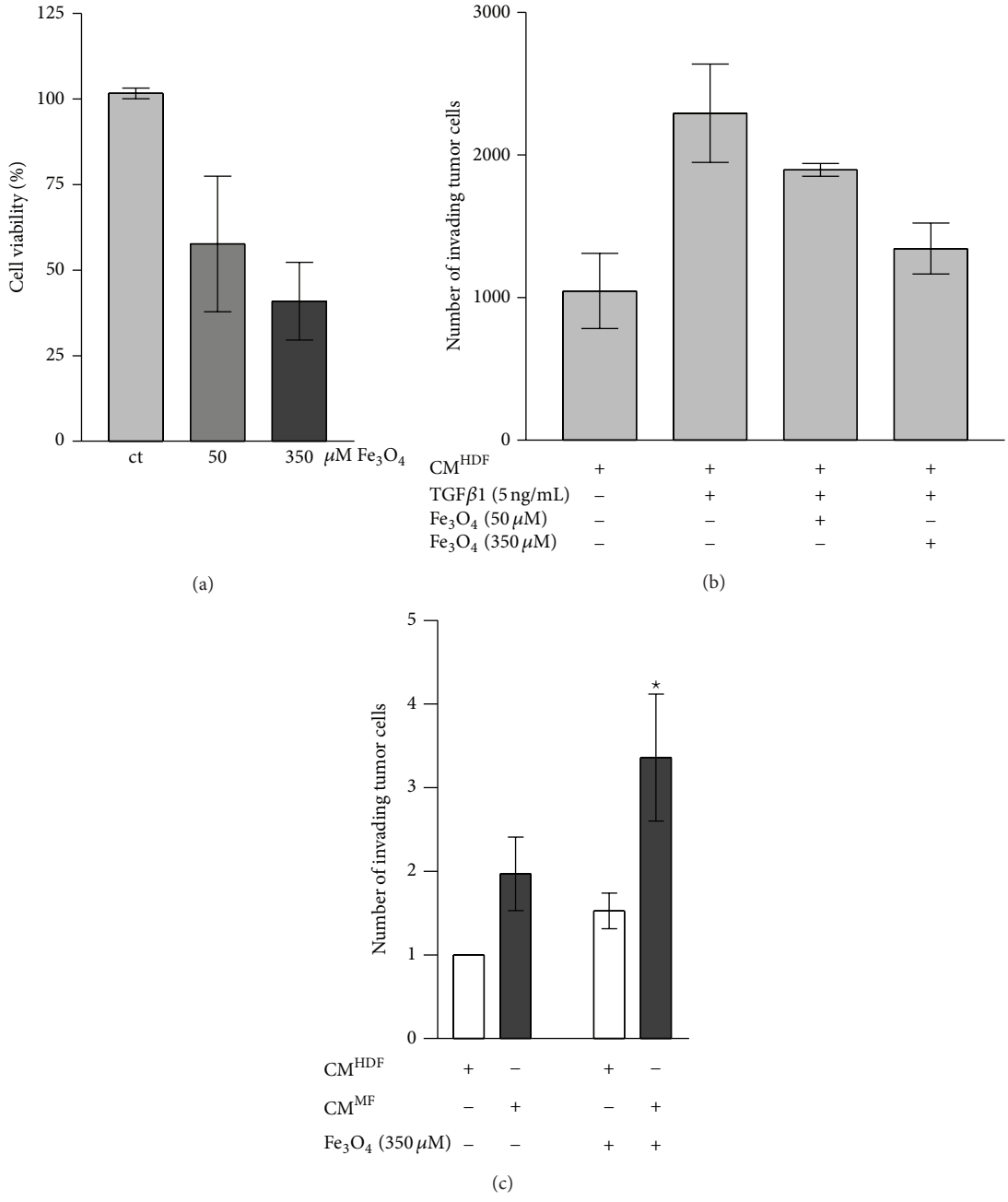

Figure 3: (a) Cell viability of SCL-1 tumor cells. Cells (SCL-1) were incubated with Fe_3O_4 nanoparticles. The percentage of living cells after 72 h was measured. $n = 3$. Ct: control (untreated). (b) Involvement of Fe_3O_4 nanoparticles in tumor invasion. Conditioned media of HDF (CM^{HDF}), myofibroblasts (CM^{MF}), and fibroblasts incubated with 50 μM or 350 μM Fe_3O_4 nanoparticles and rTGFβ1 (CM^{HDF,TGF,Fe_3O_4}) were used to check the invasive capacity of tumor cells. The data represent the mean ± s.e.m. $n = 3$. (c) Direct effect of Fe_3O_4 nanoparticles on tumor cells. SCL-1 tumor cells were untreated or incubated with 350 μm Fe_3O_4 nanoparticles for 24 h. The invasion assay was performed with conditioned media of HDF (CM^{HDF}) and myofibroblasts (CM^{MF}). The data represent the mean ± s.e.m. $n = 3$. $^*p < 0.05$ versus CM^{MF} (Student's t-test). CM: conditioned medium.

SCL-1 tumor cells was observed compared with untreated control cells, while the treatment with 350 μM Fe_3O_4 for 4 h resulted in an increase of the 8-isoprostane level. After 12 h incubation both Fe_3O_4 nanoparticle concentrations showed an about 2-fold increase of released 8-isoprostane compared with untreated cells.

3.8. Formation of Malondialdehyde by Fe_3O_4 Nanoparticles. Lipid peroxidation leads to production of malondialdehyde (MDA). MDA is an unsaturated hydroxyl aldehyde and is generated, like the isoprostanes, as one of several end products during the ROS-induced lipid peroxidation [44]. Treatment of SCL-1 cells with both Fe_3O_4 nanoparticle

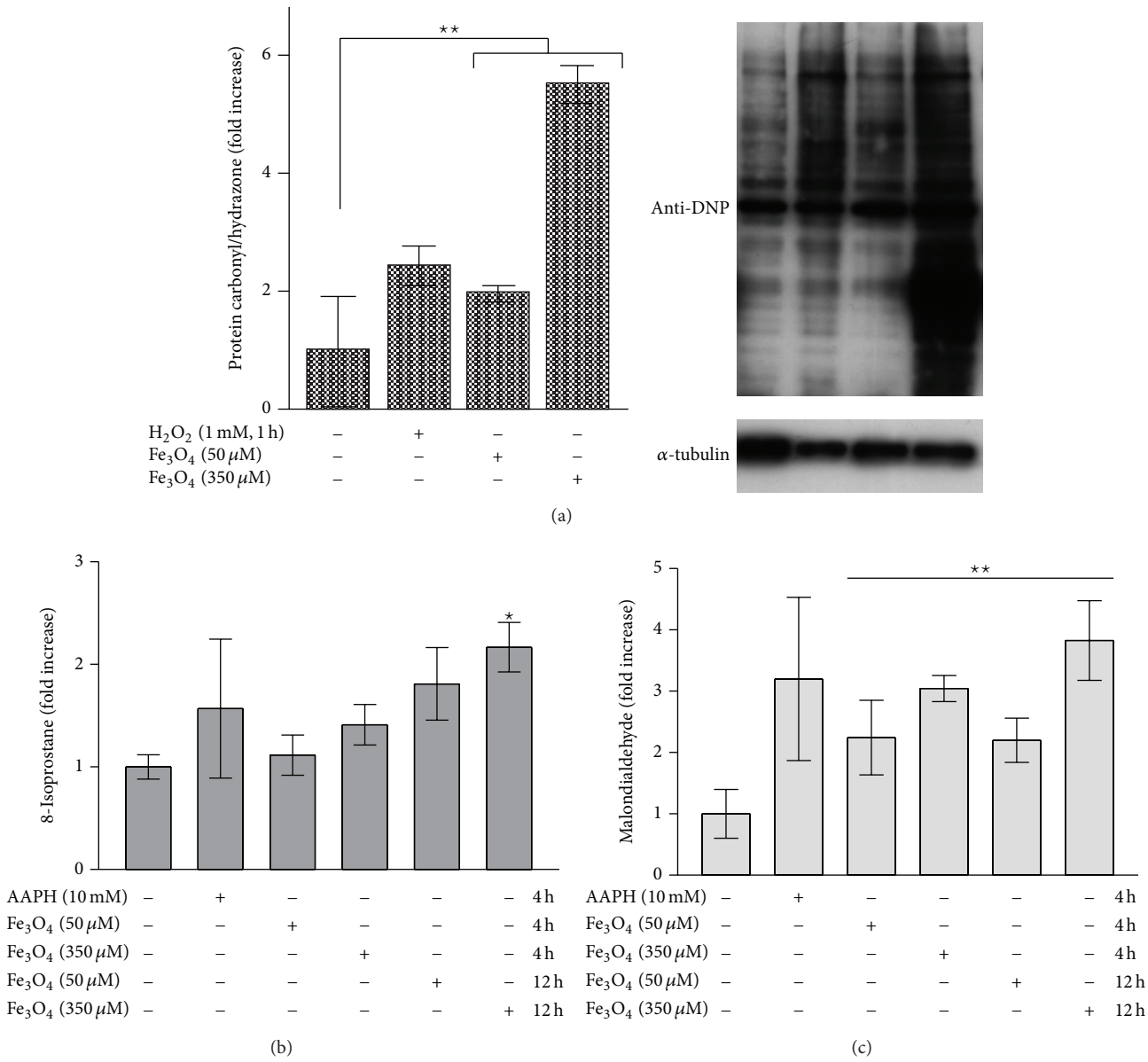

Figure 4: (a) Reactive oxygen species and carbonylated proteins. Tumor cells were untreated or incubated with 350 μM Fe_3O_4 nanoparticles for 24 h. Carbonylated proteins were evaluated by western blot analysis. 250 μM H_2O_2 was incubated for 1 h and served as positive control and α-tubulin served as loading control. $n = 3$. CM: conditioned medium. $^{**}p < 0.01$ versus untreated control (ANOVA, Dunnett's test). (b) Detection of 8-isoprostane in SCL-1 cell supernatants. Subconfluent SCL-1 cells were incubated with Fe_3O_4 nanoparticles (50 μM, 350 μM) for 4 h and 12 h and with 2,2′-azobis(2-amidinopropane) dihydrochloride (AAPH, 10 mM, radical initiator) for 4 h as a positive control. The cell culture supernatants were collected and a competitive ELISA assay applied. The 8-isoprostane concentration of untreated control was set at 1. The data represent the mean ± s.e.m. $n = 3$. $^{*}p < 0.05$ versus untreated control (CM^{SCL}) (Student's t-test). (c) MDA formation in SCL-1. MDA formation as a marker for lipid peroxidation was determined by HPLC. Subconfluent SCL-1 cells were treated with Fe_3O_4 nanoparticles (50 μM, 350 μM) for 4 h and 12 h and with AAPH (10 mM, radical initiator) for 4 h as a positive control. The data represent the fold increase over control, which was set at 1. The data represent the mean ± s.e.m. $n = 3$. $^{**}p < 0.01$ versus untreated control (ANOVA, Dunnett's test).

concentrations for 4 h led to a significant increase in the intracellular MDA content compared to untreated control cells (Figure 4(c)). Cells incubated with 50 μM Fe_3O_4 showed a 2-fold increase of MDA compared to untreated control cells, while with 350 μM Fe_3O_4 a 3-fold increase was detectable in cell lysates. After 12 h, SCL-1 cells treated with 350 μM Fe_3O_4 showed an almost 4-fold increased generation of MDA compared to untreated control cells.

Fe_3O_4 nanoparticles generate free oxygen radicals and produce significant oxidative stress in squamous tumor cells

resulting in a decrease in cell viability, but apparently increase the invasive capacity of cancer cells surviving the treatment with nanoparticles.

4. Discussion

An increasing number of different types of nanoparticles are used for applications in the biomedical field, from use as contrast agent to potential carriers for drug delivery. The possible toxic properties of nanoparticles on human health are controversially discussed [18, 47] and further studies are needed to understand and evaluate their function and more specific their toxicity.

Many publications have evaluated the biocompatibility of super paramagnetic iron oxide nanoparticles in different cell types, that is, macrophages [48], endothelial cells [49], and fibroblasts [50, 51]. Experiments on the influence of iron oxide nanoparticles in human dermal fibroblasts, representing stromal cells, and squamous cancer cells are limited.

In comparison with dextran-coated cerium oxide nanoparticles [30], the question was addressed of whether Fe_3O_4 nanoparticles have the same bifunctional character like, namely, an antioxidant effect on human dermal fibroblasts and a prooxidative effect in tumor cells.

In this study, we showed that Fe_3O_4 nanoparticles prevented TGFβ1-triggered and ROS-initiated formation of myofibroblasts. The treatment of fibroblasts with the iron nanoparticles is speculated to inhibit the secretion of proinvasive soluble factors and resulted in a significantly lowered invasion of SCL-1 cells. This data correlates with the results obtained with classical antioxidants [16] or redox-active cerium oxide nanoparticles [30, 47]. However, the direct treatment of the tumor cells with the iron nanoparticles increased the invasiveness of a fraction of that cells.

ROS production by Fe_3O_4 nanoparticles causes the cytotoxic effect in several cell types [52]. Fe_3O_4 is unstable and can easily be oxidized to yield γ-Fe_2O_3 + Fe^{2+} [53–55]. The free Fe^{2+} ions are able to produce highly reactive hydroxyl radicals ($HO^{\cdot}$, Fenton reaction) by reaction with H_2O_2 or O_2 and Fe^{3+} ions [56] that can modify proteins, lipids, and DNA [52]. Earlier studies described that Fe_3O_4 caused an increase in oxidative stress and lipid peroxidation in tumor cells, for example, skin epithelial A431 and lung epithelial A549 [57].

5. Conclusion

Fe_3O_4 particles with a mean diameter of 65 nm generated reactive oxygen species and, as a consequence, being toxic as well as proinvasive on the fraction of squamous cancer cells surviving the treatment with Fe_3O_4 nanoparticles whereas the same concentration does not alter the viability of human dermal fibroblasts which were used as model for stromal cells in skin cancer. These data are in contrast to the recently described effect of cerium oxide nanoparticles on tumor cells [30] indicating that the Fe_3O_4 nanoparticles appear not to be adequate for use in therapeutic approaches against cancer cells.

Conflict of Interests

The authors declare no competing financial interest or interest otherwise.

Acknowledgments

This work is part of the master thesis of Swetlana Chapiro at the Heinrich Heine University of Düsseldorf. The authors thank C. Wyrich and V. Pützer for her excellent technical assistance.

References

[1] L. A. Liotta and W. G. Stetler-Stevenson, "Tumor invasion and metastasis: an imbalance of positive and negative regulation," *Cancer Research*, vol. 51, no. 18, supplement, pp. 5054s–5059s, 1991.

[2] J. Sleeman and P. S. Steeg, "Cancer metastasis as a therapeutic target," *European Journal of Cancer*, vol. 46, no. 7, pp. 1177–1180, 2010.

[3] M. M. Mueller and N. E. Fusenig, "Tumor-stroma interactions directing phenotype and progression of epithelial skin tumor cells," *Differentiation*, vol. 70, no. 9-10, pp. 486–497, 2002.

[4] O. de Wever and M. Mareel, "Role of tissue stroma in cancer cell invasion," *Journal of Pathology*, vol. 200, no. 4, pp. 429–447, 2003.

[5] L. A. Liotta and E. C. Kohn, "The microenvironment of the tumour—host interface," *Nature*, vol. 411, no. 6835, pp. 375–379, 2001.

[6] L. A. Kunz-Schughart and R. Knuechel, "Tumor-associated fibroblasts (Part II): functional impact on tumor tissue," *Histology and Histopathology*, vol. 17, no. 2, pp. 623–637, 2002.

[7] G. Gabbiani, G. B. Ryan, and G. Majno, "Presence of modified fibroblasts in granulation tissue and their possible role in wound contraction," *Cellular and Molecular Life Sciences*, vol. 27, no. 5, pp. 549–550, 1971.

[8] G. Majno, G. Gabbiani, B. J. Hirschel, G. B. Ryan, and P. R. Statkov, "Contraction of granulation tissue in vitro: similarity to smooth muscle," *Science*, vol. 173, no. 3996, pp. 548–550, 1971.

[9] A. Desmoulière, C. Guyot, and G. Gabbiani, "The stroma reaction myofibroblast: a key player in the control of tumor cell behavior," *International Journal of Developmental Biology*, vol. 48, no. 5-6, pp. 509–517, 2004.

[10] W. Schürch, T. A. Seemayer, and G. Gabbiani, "The myofibroblast: a quarter century after its discovery," *The American Journal of Surgical Pathology*, vol. 22, no. 2, pp. 141–147, 1998.

[11] D. W. Powell, R. C. Mifflin, J. D. Valentich, S. E. Crowe, J. I. Saada, and A. B. West, "Myofibroblasts. I. Paracrine cells important in health and disease," *The American Journal of Physiology—Cell Physiology*, vol. 277, no. 1, pp. C1–C19, 1999.

[12] O. De Wever, Q.-D. Nguyen, L. Van Hoorde et al., "Tenascin-C and SF/HGF produced by myofibroblasts in vitro provide convergent pro-invasive signals to human colon cancer cells through RhoA and Rac," *The FASEB Journal*, vol. 18, no. 9, pp. 1016–1018, 2004.

[13] O. De Wever, P. Demetter, M. Mareel, and M. Bracke, "Stromal myofibroblasts are drivers of invasive cancer growth," *International Journal of Cancer*, vol. 123, no. 10, pp. 2229–2238, 2008.

[14] W. Ishida, Y. Mori, G. Lakos et al., "Intracellular TGF-β receptor blockade abrogates smad-dependent fibroblast activation *in*

vitro and *in vivo*," *Journal of Investigative Dermatology*, vol. 126, no. 8, pp. 1733–1744, 2006.

[15] R. Derynck and Y. E. Zhang, "Smad-dependent and Smad-independent pathways in TGF-beta family signalling," *Nature*, vol. 425, no. 6958, pp. 577–584, 2003.

[16] B. Cat, D. Stuhlmann, H. Steinbrenner et al., "Enhancement of tumor invasion depends on transdifferentiation of skin fibroblasts mediated by reactive oxygen species," *Journal of Cell Science*, vol. 119, part 13, pp. 2727–2738, 2006.

[17] L. Alili, M. Sack, K. Puschmann, and P. Brenneisen, "Fibroblast-to-myofibroblast switch is mediated by NAD(P)H oxidase generated reactive oxygen species," *Bioscience Reports*, vol. 34, no. 1, Article ID e00089, 2014.

[18] M. Auffan, J. Rose, J.-Y. Bottero, G. V. Lowry, J.-P. Jolivet, and M. R. Wiesner, "Towards a definition of inorganic nanoparticles from an environmental, health and safety perspective," *Nature Nanotechnology*, vol. 4, no. 10, pp. 634–641, 2009.

[19] J. M. Perez, "Iron oxide nanoparticles: hidden talent," *Nature Nanotechnology*, vol. 2, no. 9, pp. 535–536, 2007.

[20] J. Klein, "Probing the interactions of proteins and nanoparticles," *Proceedings of the National Academy of Sciences of the United States of America*, vol. 104, no. 7, pp. 2029–2030, 2007.

[21] M. Simkó, "Cell type specific redox status is responsible for diverse electromagnetic field effects," *Current Medicinal Chemistry*, vol. 14, no. 10, pp. 1141–1152, 2007.

[22] C. Boyer, M. R. Whittaker, V. Bulmus, J. Liu, and T. P. Davis, "The design and utility of polymer-stabilized iron-oxide nanoparticles for nanomedicine applications," *NPG Asia Materials*, vol. 2, no. 1, pp. 23–30, 2010.

[23] A. Jordan, R. Scholz, K. Maier-Hauff et al., "Presentation of a new magnetic field therapy system for the treatment of human solid tumors with magnetic fluid hyper-thermia," *Journal of Magnetism and Magnetic Materials*, vol. 225, no. 1-2, pp. 118–126, 2001.

[24] G. L. DeNardo and S. J. DeNardo, "Turning the heat on cancer," *Cancer Biotherapy & Radiopharmaceuticals*, vol. 23, no. 6, pp. 671–679, 2008.

[25] J. Dobson, "Cancer therapy: a twist on tumour targeting," *Nature Materials*, vol. 9, no. 2, pp. 95–96, 2010.

[26] E. G. Heckert, A. S. Karakoti, S. Seal, and W. T. Self, "The role of cerium redox state in the SOD mimetic activity of nanoceria," *Biomaterials*, vol. 29, no. 18, pp. 2705–2709, 2008.

[27] S. M. Hirst, A. S. Karakoti, R. D. Tyler, N. Sriranganathan, S. Seal, and C. M. Reilly, "Anti-inflammatory properties of cerium oxide nanoparticles," *Small*, vol. 5, no. 24, pp. 2848–2856, 2009.

[28] A. Karakoti, S. Singh, J. M. Dowding, S. Seal, and W. T. Self, "Redox-active radical scavenging nanomaterials," *Chemical Society Reviews*, vol. 39, no. 11, pp. 4422–4432, 2010.

[29] G. Oberdörster, Z. Sharp, V. Atudorei et al., "Translocation of inhaled ultrafine particles to the brain," *Inhalation Toxicology*, vol. 16, no. 6-7, pp. 437–445, 2004.

[30] L. Alili, M. Sack, A. S. Karakoti et al., "Combined cytotoxic and anti-invasive properties of redox-active nanoparticles in tumor-stroma interactions," *Biomaterials*, vol. 32, no. 11, pp. 2918–2929, 2011.

[31] T. Pirmohamed, J. M. Dowding, S. Singh et al., "Nanoceria exhibit redox state-dependent catalase mimetic activity," *Chemical Communications*, vol. 46, no. 16, pp. 2736–2738, 2010.

[32] K. Bayreuther, P. I. Francz, J. Gogol, and K. Kontermann, "Terminal differentiation, aging, apoptosis, and spontaneous transformation in fibroblast stem cell systems in vivo and in vitro," *Annals of the New York Academy of Sciences*, vol. 663, pp. 167–179, 1992.

[33] P. Boukamp, W. Tilgen, R. T. Dzarlieva et al., "Phenotypic and genotypic characteristics of a cell line from a squamous cell carcinoma of human skin," *Journal of the National Cancer Institute*, vol. 68, no. 3, pp. 415–427, 1982.

[34] D. Stuhlmann, N. Ale-Agha, R. Reinehr et al., "Modulation of homologous gap junctional intercellular communication of human dermal fibroblasts via a paracrine factor(s) generated by squamous tumor cells," *Carcinogenesis*, vol. 24, no. 11, pp. 1737–1748, 2003.

[35] R. Massart and V. Cabuil, "Effect of some parameters on the formation of colloidal magnetite in alkaline medium: yield and particle size control," *Journal de Chimie Physique*, vol. 84, no. 7-8, pp. 967–973, 1987.

[36] G. U. Marten, T. Gelbrich, and A. M. Schmidt, "Hybrid biofunctional nanostructures as stimuli-responsive catalytic systems," *Beilstein Journal of Organic Chemistry*, vol. 6, pp. 922–931, 2010.

[37] T. Mosmann, "Rapid colorimetric assay for cellular growth and survival: application to proliferation and cytotoxicity assays," *Journal of Immunological Methods*, vol. 65, no. 1-2, pp. 55–63, 1983.

[38] E. S. Reynolds, "The use of lead citrate at high pH as an electron-opaque stain in electron microscopy," *Journal of Cell Biology*, vol. 17, pp. 208–212, 1963.

[39] U. K. Laemmli, "Cleavage of structural proteins during the assembly of the head of bacteriophage T4," *Nature*, vol. 227, no. 5259, pp. 680–685, 1970.

[40] A. Junghans, H. Sies, and W. Stahl, "Carotenoid-containing unilamellar liposomes loaded with glutathione: a model to study hydrophobic-hyrophilic antioxidant interaction," *Free Radical Research*, vol. 33, no. 6, pp. 801–808, 2000.

[41] Z. A. Placer, L. L. Cushman, and B. C. Johnson, "Estimation of product of lipid peroxidation (malonyl dialdehyde) in biochemical systems," *Analytical Biochemistry*, vol. 16, no. 2, pp. 359–364, 1966.

[42] S. Wagener, T. Völker, S. de Spirt, H. Ernst, and W. Stahl, "3,3*ı*-Dihydroxyisorenieratene and isorenieratene prevent UV-induced DNA damage in human skin fibroblasts," *Free Radical Biology and Medicine*, vol. 53, no. 3, pp. 457–463, 2012.

[43] L.-J. Yan and M. J. Forster, "Chemical probes for analysis of carbonylated proteins: a review," *Journal of Chromatography B: Analytical Technologies in the Biomedical and Life Sciences*, vol. 879, no. 17-18, pp. 1308–1315, 2011.

[44] K. Moore and L. J. Roberts II, "Measurement of lipid peroxidation," *Free Radical Research*, vol. 28, no. 6, pp. 659–671, 1998.

[45] J. D. Morrow, Y. Chen, C. J. Brame et al., "The isoprostanes: unique prostaglandin-like products of free-radical- initiated lipid peroxidation," *Drug Metabolism Reviews*, vol. 31, no. 1, pp. 117–139, 1999.

[46] L. J. Roberts II and J. D. Morrow, "Measurement of F_2-isoprostanes as an index of oxidative stress in vivo," *Free Radical Biology and Medicine*, vol. 28, no. 4, pp. 505–513, 2000.

[47] L. Alili, M. Sack, C. von Montfort et al., "Downregulation of tumor growth and invasion by redox-active nanoparticles," *Antioxidants and Redox Signaling*, vol. 19, no. 8, pp. 765–778, 2013.

[48] I. Siglienti, M. Bendszus, C. Kleinschnitz, and G. Stoll, "Cytokine profile of iron-laden macrophages: implications for cellular magnetic resonance imaging," *Journal of Neuroimmunology*, vol. 173, no. 1-2, pp. 166–173, 2006.

[49] A. Moore, E. Marecos, A. Bogdanov Jr., and R. Weissleder, "Tumoral distribution of long-circulating dextran-coated iron oxide nanoparticles in a rodent model," *Radiology*, vol. 214, no. 2, pp. 568–574, 2000.

[50] C. C. Berry, S. Wells, S. Charles, G. Aitchison, and A. S. G. Curtis, "Cell response to dextran-derivatised iron oxide nanoparticles post internalisation," *Biomaterials*, vol. 25, no. 23, pp. 5405–5413, 2004.

[51] C. C. Berry, S. Wells, S. Charles, and A. S. G. Curtis, "Dextran and albumin derivatised iron oxide nanoparticles: influence on fibroblasts in vitro," *Biomaterials*, vol. 24, no. 25, pp. 4551–4557, 2003.

[52] M. Watanabe, M. Yoneda, A. Morohashi et al., "Effects of Fe_3O_4 magnetic nanoparticles on A549 cells," *International Journal of Molecular Sciences*, vol. 14, no. 8, pp. 15546–15560, 2013.

[53] N. Singh, G. J. Jenkins, R. Asadi, and S. H. Doak, "Potential toxicity of superparamagnetic iron oxide nanoparticles (SPION)," *Nano Reviews*, vol. 1, article 5358, 2010.

[54] J.-E. Kim, J.-Y. Shin, and M.-H. Cho, "Magnetic nanoparticles: an update of application for drug delivery and possible toxic effects," *Archives of Toxicology*, vol. 86, no. 5, pp. 685–700, 2012.

[55] E. Birben, U. M. Sahiner, C. Sackesen, S. Erzurum, and O. Kalayci, "Oxidative stress and antioxidant defense," *World Allergy Organization Journal*, vol. 5, no. 1, pp. 9–19, 2012.

[56] D. A. Tulis, W. Durante, X. Liu, A. J. Evans, K. J. Peyton, and A. I. Schafer, "Adenovirus-mediated heme oxygenase-1 gene delivery inhibits injury-induced vascular neointima formation," *Circulation*, vol. 104, no. 22, pp. 2710–2715, 2001.

[57] M. Ahamed, H. A. Alhadlaq, J. Alam, M. A. Majeed Khan, D. Ali, and S. Alarafi, "Iron oxide nanoparticle-induced oxidative stress and genotoxicity in human skin epithelial and lung epithelial cell lines," *Current Pharmaceutical Design*, vol. 19, no. 37, pp. 6681–6690, 2013.